ELSEVIER

Journal of Nuclear Materials 290–293 (2001) 940–946

journal of nuclear materials

www.elsevier.nl/locate/jnucmat

Divertor geometry effects on detachment in TCV

R.A. Pitts [a,*], B.P. Duval [a], A. Loarte [b], J.-M. Moret [a], J.A. Boedo [c], D. Coster [d], I. Furno [a], J. Horacek [e], A.S. Kukushkin [f], D. Reiter [g], J. Rommers [a], The TCV Team [1]

[a] *Centre de Recherches en Physique des Plasmas, Association EURATOM-Confédération Suisse, École Polytechnique Fédérale de Lausanne, CH-1015 Lausanne, Switzerland*

[b] *EFDA-CSU, Max Planck Institut für Plasmaphysik, D-85748 Garching, Germany*

[c] *Fusion Energy Program, University of California, San Diego, CA 92093-0417, USA*

[d] *Max-Plank-Insitut für Plasmaphysik, Boltzmannstr. 2, D-85748 Garching, Germany*

[e] *IPP, Academy of Sciences of the Czech Republic, Za Slovankou 3, P.O. Box 17, 182 21 Czech Republic*

[f] *ITER Joint Central Team, Garching Joint Working Site, Boltzmannstr. 2, D-85748 Garching, Germany*

[g] *Institut für Laser und Plasmaphysik, Heinrich-Heine-Universität Düsseldorf, Universitätsstr.1, D-40225 Düsseldorf, Germany*

Abstract

Experimental observations and some preliminary results from B2-Eirene code modelling of divertor detachment in the TCV tokamak are reported, with emphasis on the aspects of this detachment related to divertor geometry. The contribution is restricted to deuterium fuelled, ohmic plasmas for which the ∇B drift is directed away from the X-point of lower single-null, open diverted equilibria with fixed elongation and triangularity. Unlike more conventional diverted equilibria, however, the configurations described are characterised by both a very short divertor poloidal depth on a vertical target and a very long poloidal depth on a horizontal target. Results are presented from density ramp discharges in which the outer (high poloidal depth) divertor is already in the high recycling regime at the start of the density ramp and in which varying degrees of detachment are obtained depending on the magnitude of the imposed outer divertor flux expansion. In contrast, the inner divertor remains in the large part attached for all densities.

Keywords: Divertor detachment; TCV; Edge plasma; Geometry effect; Langmuir probe

1. Introduction

The existing coil set and first wall design impose short X-point to central column distances for diverted discharges created in the TCV tokamak ($R = 0.89$ m, $a = 0.25$ m, $B_\varphi = 1.43$ T). In turn, this requires that at least one of the divertor legs in single-null equilibria be poloidally rather short, although considerable freedom exists for modifying the magnetic geometry of the low field side (LFS) divertor leg. One particular configuration is used as a base for divertor physics studies in TCV (see Fig. 1) and was presented in an earlier paper in connection with detachment studies using neon seeding [2]. Following the TCV first wall upgrade in late 1998 [3], in which the coverage of carbon protection tiles was increased from ≈65% to ≈90% of internal surface area, detachment has been observed with D_2 fuelling alone. This contribution presents some of the first experimental observations of this detachment, with particular emphasis on the role of outer divertor geometry. The results of some preliminary simulations of the experiments using the B2-Eirene code package are also reported.

2. Experiment

Fig. 1 summarises the the typical density ramp discharge used to investigate detachment and illustrates the

* Corresponding author. Tel.: +44-21 693 60 03; fax: +44-21 693 5176.

E-mail address: richard.pitts@eplf.ch (R.A. Pitts).

[1] For the full list of authors see, for example [1].

0022-3115/01/$ - see front matter
PII: S0022-3115(00)00461-X

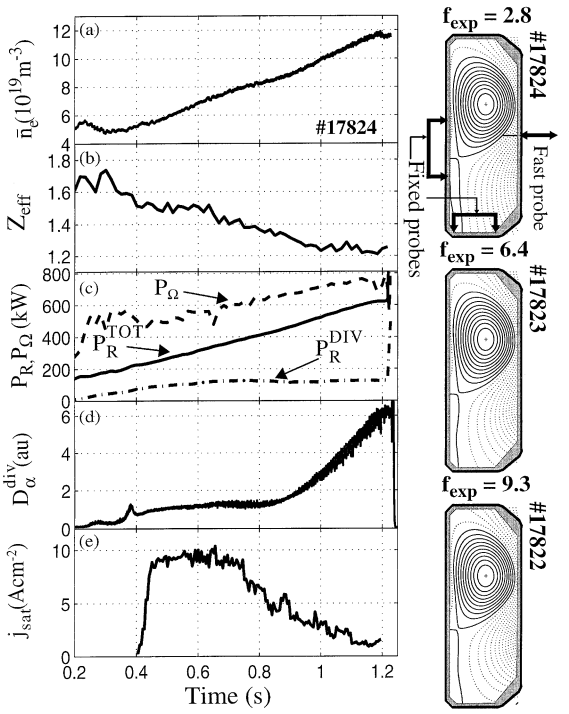

Fig. 1. Time variation of some relevant plasma signals for a typical density ramp detachment discharge. The equilibria to the right illustrate the range of outer divertor flux expansion investigated in this study. The location of Langmuir probe diagnostics is also indicated. All equilibria plotted at $t = 0.8$ s.

three equilibria discussed in this contribution. All have $\kappa_{95} = 1.6$, $\delta_{95} = 0.35$ and fixed X-point height, $z_{X\mathrm{pt}} = 57$ cm, defined as the vertical distance from the X-point to the vessel floor. The emphasis here is on the effect of outer divertor flux expansion, f_{exp}, the values of which close to the separatrix are noted in the figure for the specific discharges and which fall in the general range $f_{\mathrm{exp}} = 2.5 \rightarrow 10$ for all shots of this type executed thus far. This should be compared with the value at the inner target, fixed at 4.0 for all equilibria. Experiments have been performed in ohmic plasmas only with $B \times \nabla B$ drift direction away from the X-point and plasma current, $I_{\mathrm{p}} = 340$ kA, corresponding to $q_{95} = 2.9$. Under these conditions, the midplane to outer target parallel connection length near the separatrix is $\approx$25 m with $\approx$70% of this appearing in the poloidal distance, $z_{X\mathrm{pt}}$. In contrast, the inner X-point to target poloidal distance is only some 8 cm, corresponding to only $\approx$2.5 m parallel to the total field. An interesting feature of these configurations is the unavoidable presence in the same discharge of both a horizontal and a vertical target zone.

Much of the data discussed here originate from two arrays of single Langmuir probes and a fast reciprocating probe, the positions of which are also indicated in Fig. 1. The divertor target arrays comprise 26 and 34 spherical tips, cylindrical graphite single probes of diameter 4.0 mm, embedded in the outer and inner target tiles and with spatial resolutions of 11.0 and 17.0 mm, respectively. The fast probe [4] enters the plasma edge at the tokamak midplane and makes two reciprocations per discharge, with the peak of the first movement at the beginning of the density ramp and the second when detachment has begun at the outer target.

The observed detachment has most of the characteristics seen under similar conditions in other devices [5–8]. All of the examples described here terminate in disruption when $\bar{n}_{\mathrm{e}} \approx 65\%$ of the Greenwald limit and the ratio $P_{\mathrm{R}}^{\mathrm{TOT}}/P_{\Omega} \approx 0.8$ (Fig. 1(c)). This does not, however, appear to be specifically linked to any particular movement of the radiation distribution around the X-point which, from relatively early on in the density ramp is localised at the X-point. In fact, in most cases, the disruption occurs a few tens of ms after the current plateau when the outer divertor leg is beginning to move back up the central column (although the density is still rising). The divertor radiation, $P_{\mathrm{R}}^{\mathrm{DIV}}$, saturates quickly after the density ramp begins, corresponding to the establishment of a high recycling regime at the outer target (note in Fig. 1(e) the plateau on the ion saturation current density of a probe located close to the outer strike point). This is simply due to the low temperatures established throughout the divertor volume, such that most of the radiation originates from the X-point region, where T_{e} is sufficiently high for carbon to radiate strongly. At around 0.75 s, when, for this particular dicharge, $\bar{n}_{\mathrm{e}} = 7.5 \times 10^{19}$ m^{-3}, the separatrix target ion flux begins to fall, and shortly afterward the D_α emission in the region near the outer target (Fig. 1(d)) begins to increase rapidly. One may also note the extremely low core average Z_{eff} of these plasmas (Fig. 1(b)), and in particular, the steady decrease in Z_{eff} as $\bar{n}_{\mathrm{e}}$ increases and detachment proceeds.

3. Divertor and SOL measurements

3.1. Target probes

Ion fluxes to the target probes can be used to compute a degree of detachment (DOD) [5], describing the extent to which the ion flux obeys the scaling, $\Gamma \propto \bar{n}_{\mathrm{e}}^2$ predicted by the basic Two-Point Model [9] of the divertor for the high recycling regime. These DODs have been computed at both targets for the separatrix ion current density and the integrated ion current normal to the tiles across the strike zones. Fig. 2 collects the results for three values of f_{exp}. When the DOD $\gg 1$, detachment is occurring and one may note that at lower f_{exp}, separatrix detachment occurs rapidly and is quickly complete, whilst with increasing f_{exp}, the separatix DOD

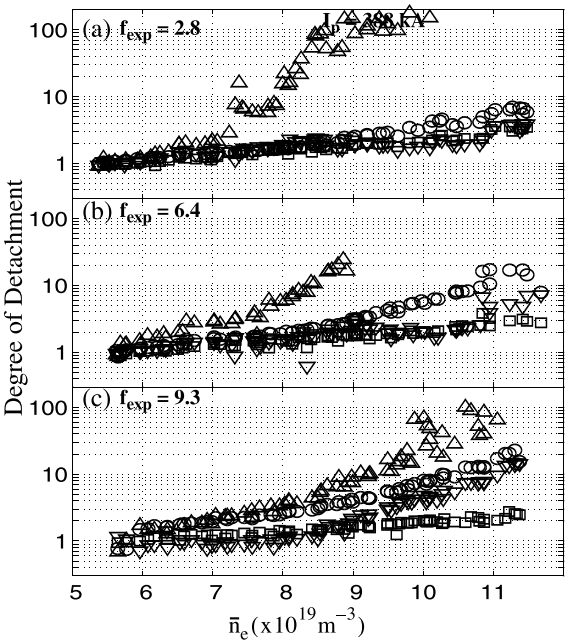

Fig. 2. Degree of separatrix and integral ion flux detachment for both inner and outer divertor targets. The symbols have the following meaning: (○) outer divertor, integral current; (□) inner divertor, integral current; (Δ), outer divertor, separatrix current density; (▽), inner divertor, separatrix current density.

reaches lower values and does so more slowly. In the meantime, the integral DODs increase with f_{exp} indicating the greater extent of detachment at higher flux expansion. At the inner target, except at the very highest $\bar{n}_e$ and close to the separatrix, the plasma remains attached throughout, with separatrix particle flux densities a factor of 3–3.5 higher than those at the outer target, independent of flux expansion.

3.2. Reciprocating probe

Fig. 3 combines target and reciprocating probe profiles of electron density, temperature and pressure mapped to the outer midplane for the equilibrium with lowest f_{exp}. The profiles are plotted in terms of distance from the magnetically located separatrix position, with the target profiles as the result of averaging over 30 ms, centred on the time of maximum insertion point during the fast probe reciprocation. The earlier time corresponds to high recycling with $\bar{n}_e = 7 \times 10^{19}$ m^{-3} and the second movement at 1.0 s to $\bar{n}_e = 1 \times 10^{20}$ m^{-3} when detachment is well advanced.

An immediately obvious feature is the SOL density broadening during detachment and the apparent shift of the peak in the inner target T_e profile at high density. One may also note the abrupt change in gradient of all signals at the location of the dashed vertical lines. The latter indicate the outer wall tile radius at the midplane so that data points at radii exceeding this location correspond to plasma on field lines intersecting the outer wall before arriving at the midplane.

Within experimental errors, pressure balance appears to be reasonably satisfied during high recycling and detachment at the inner target but not at higher density for the outer target, as might be expected. It is significant, however, that outer target densities during detachment are considerably lower than the upstream values, whilst downstream and upstream temperatures are similar. Since $\bar{n}_e \propto 1/\sqrt{T_e}$, this leads one naturally to speculate on the validity of the T_e obtained from these divertor probes under such conditions, particularly in view of the code results presented in Section 4 showing that the local T_e is considerably lower than that measured. Such a speculation is nothing new [10,11] and there are strong arguments for the case of the TCV divertor in support of significant deviations of the measured T_e from the real value local to the outer target under detached conditions [12].

3.3. Visible emission reconstructions

In recent years two-dimensional measurements of visible line radiation using CCD camera technology have become increasingly popular [13]. After suitable inversion [14], the resulting distributions offer interesting insight into the dynamics and localisation of the radiation and are useful for comparison with 2D code simulations. The system on TCV [14] tangentially views the lower half of the vacuum vessel encompassing both divertor strike zones and permits observations of D_α emission at 656 nm and CIII emission at 465 nm.

The behaviour of CIII emission during the density ramp experiments described here is consistent with simple expectations based on cooling of the divertor volume with increasing $\bar{n}_e$. It is independent of f_{exp} and two examples, at the beginning and end of the density ramp for a discharge with $f_{exp} = 2.5$, are shown in Fig. 4(a) and (b). At low $\bar{n}_e$, the emission extends almost to the outer target and is most intense at the inner strike zone, where T_e and presumably carbon sputtering are higher. At the highest $\bar{n}_e$, the emission is concentrated on or just inside the outer separatrix and to a lesser extent near the X-point. This separatrix distribution is qualitatively expected to be based on the magnitude of T_e measured by the fast reciprocating probe (Fig. 3) in this region (the maximum in CIII emission should occur in regions, where $T_e \approx 8$ eV).

In the case of the D_α emission, Figs. 4(c), (d) and (f) illustrate the spatial distributions observed as f_{exp} increases. To isolate any geometry effects, such a comparison must be made on the basis of a similar DOD. This has been performed by using the experimental outer target integral DOD curves of Fig. 2 and

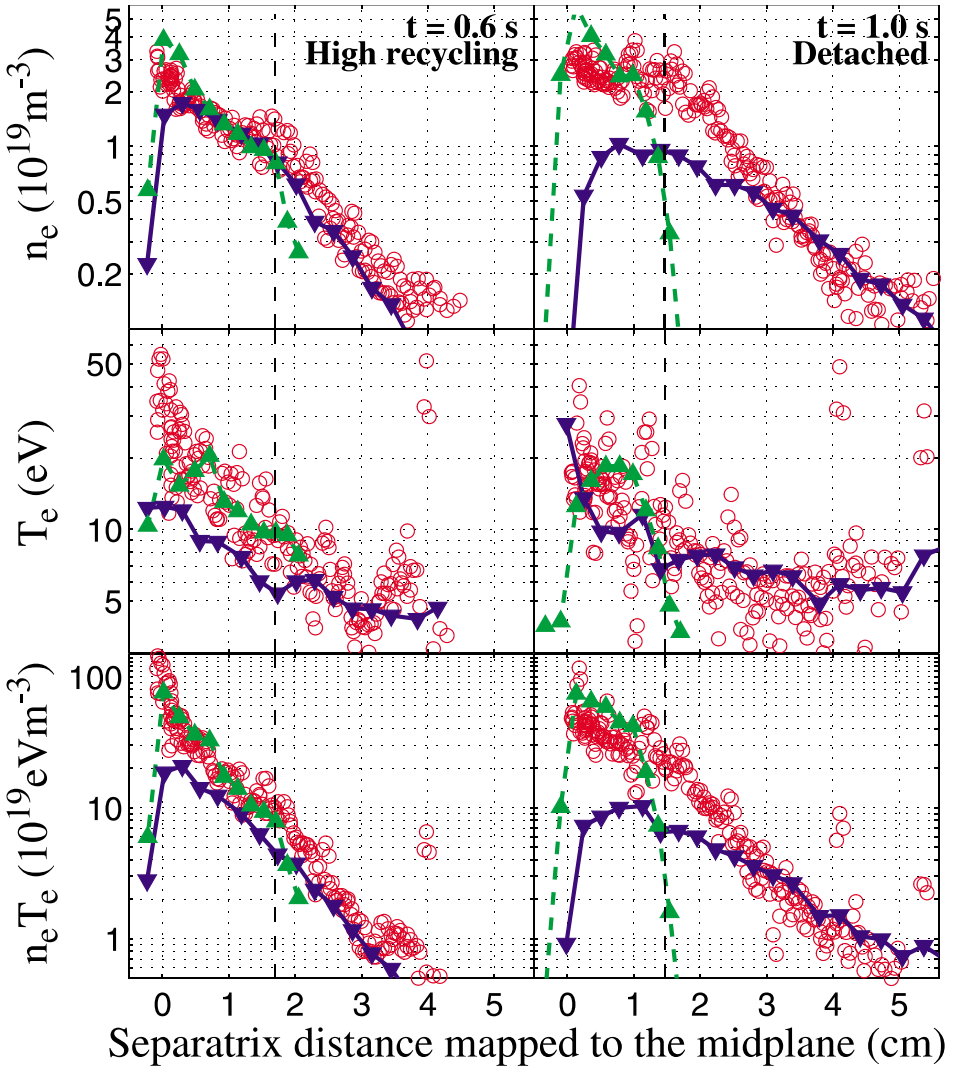

Fig. 3. Profiles of n_e, T_e and p_e for both the divertor probe arrays and the reciprocating probe at low outer divertor f_{exp} (TCV shot #17824). The data are plotted in terms of distance from the separatrix mapped to the outer midplane. Red circles: reciprocating probe, blue full line: outer target probes, green dashed line: inner target probes. The triangle symbols mark the position of the indivdual divertor probes. The vertical dashed lines locate the outer wall tile radius at the midplane.

extracting the DOD (≈60) found at highest $\bar{n}_e$ for the lowest f_{exp}. The reconstructions plotted at higher f_{exp} are thus extracted from inversions made at the densities corresponding to this value. Such a normalisation clearly shows that for lower f_{exp}, the emission extends to considerable vertical distances above the target but remains localised at the target for higher flux expansion. One may also note the apparent shift of the peak target intensity away from the separatrix as f_{exp} increases. Within the errors of CCD camera misalignment and the uncertainty in flux surface positions from the equilibrium reconstruction, the peak in the D_α profile along the target approximately coincides with that of the parallel ion flux density measured by the target probes at all values of f_{exp}. The reconstructions clearly demonstrate the effect of 'plasma plugging' by the expanded flux surfaces as f_{exp} increases.

4. Comparison with B2-Eirene code simulations

Preliminary attempts at simulating the data presented in Section 3 have concentrated on just two values of outer target flux expansion with $f_{exp} = 2.8$ and 6.4. The simulations have been performed using the B2-Eirene code [15] on TCV discharge numbers #15445 and

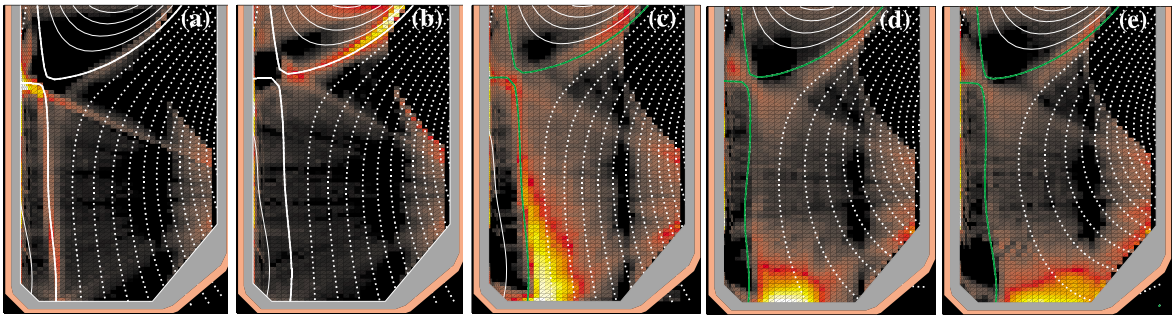

Fig. 4. Visible CCD camera inversions of D_α (656 nm) and CIII (465 nm) emissivity in the divertor region. For the CIII emission the behaviour is independent of outer target flux expansion and examples from both the beginning and end of the density ramp (a,b) serve to illustrate how the difference in temperature distribution from high recycling to detached states influences the distribution of carbon radiation. In the case of the D_α (c,d,e), a single reconstruction from each flux expansion is shown at the time of discharge for which outer target integral DODs are similar (see text). The emission is uncalibrated, but is plotted within each group of images (CIII and D_α) on the same intensity scale for ease of comparison.

#15448, identical in all respects to #17824 and #17823 of Fig. 1, respectively, with the only difference being the availability of inner target and reciprocating probe data for the later shots. As a first approximation, the power crossing the separatrix has been fixed at 0.48 MW for all densities and for both equilibria. Likewise, a chemical sputtering yield, $Y_{\mathrm{chem}} = 1.5\%$, has been chosen, arbitrarily, with $D_\perp = 0.35$ m^2 s^{-1} and $\chi_\perp = 0.85$ m^2 s^{-1} providing a reasonable agreement with the target profile shapes. Such parameters tend to overestimate the measured target ion fluxes, but this is the likely choice of a too low Y_{chem}, since a higher value would lead to more radiation for a given density, less energy available for ionisation and hence lower target currents. No inward pinch has been applied in the code and no drifts are included.

The initial code runs have highlighted the importance, in the case of TCV, of elastic friction between D_2 molecules and D^+ ions [16] which serves to slow down ions sufficiently in the region between the ionisation front and the target such that significant recombination can occur. Without this additional momentum loss (along with that due to to ion-neutral charge-exchange), the relatively low densities in the TCV divertor would not produce enough recombination to explain the observed detachment. With this effect switched on, the code yields ≈80% recombination of the target ion flux at the highest densities (before a MARFE appears in the simulation) for high f_{exp}, but is not yet able to account for the level of detachment seen experimentally at low f_{exp}.

A selection of code results is summarised in Fig. 5, with the emphasis on direct comparison with the experimental data presented in Section 3. The computed distributions of D_α line emission (due both to excitation and recombination) appear in Figs. 5(a) and (b) for low and high f_{exp}, respectively, showing very reasonable agreement with the measured spatial distributions of Fig. 4(c) and (d). In similar fashion to the experimental data, the code distributions are presented for the same absolute levels of total recombination. There is particularly striking agreement between theory and experiment with regard to the differences in vertical extent of the emission in passing from low to high f_{exp}. The indications are that this is likely due to more uniform distribution of momentum losses further up the outer leg owing to the greater neutral transparency of a laterally 'thinner' divertor. Good agreement is also obtained between the code and experiment with regard to the movement of the CIII light emission as detachment progresses, independent of flux expansion. Similarly, the absolute value and dependence on density of Z_{eff} (Fig. 1(b)) are well matched by the simulations.

Code and experiment differ, however, with respect to the localisation of D_α emission at the target. Whilst the simulation places the highest intensity at the strike point and even into the private region, experiment shows the emission to be localised further out in the divertor fan, especially at high f_{exp}. This behaviour is not currently understood, but one might speculate as to the relative importance of molecular effects in the process of detachment, even though preliminary, stand-alone Eirene simulations including a more refined treatment of deuterium molecules seem to indicate that their role might actually be in reducing the predicted level of recombination (see also [17]).

Fig. 5(c) presents the code results for the integral and separatrix DOD at low and high f_{exp} for direct comparison with Fig. 2(a) and (b). Agreement in absolute value is excellent, but, interestingly, the code is unable to reproduce the very high separatrix DOD seen experimentally at low f_{exp}. Theory does, however, correctly simulate the generally higher DODs at high f_{exp}.

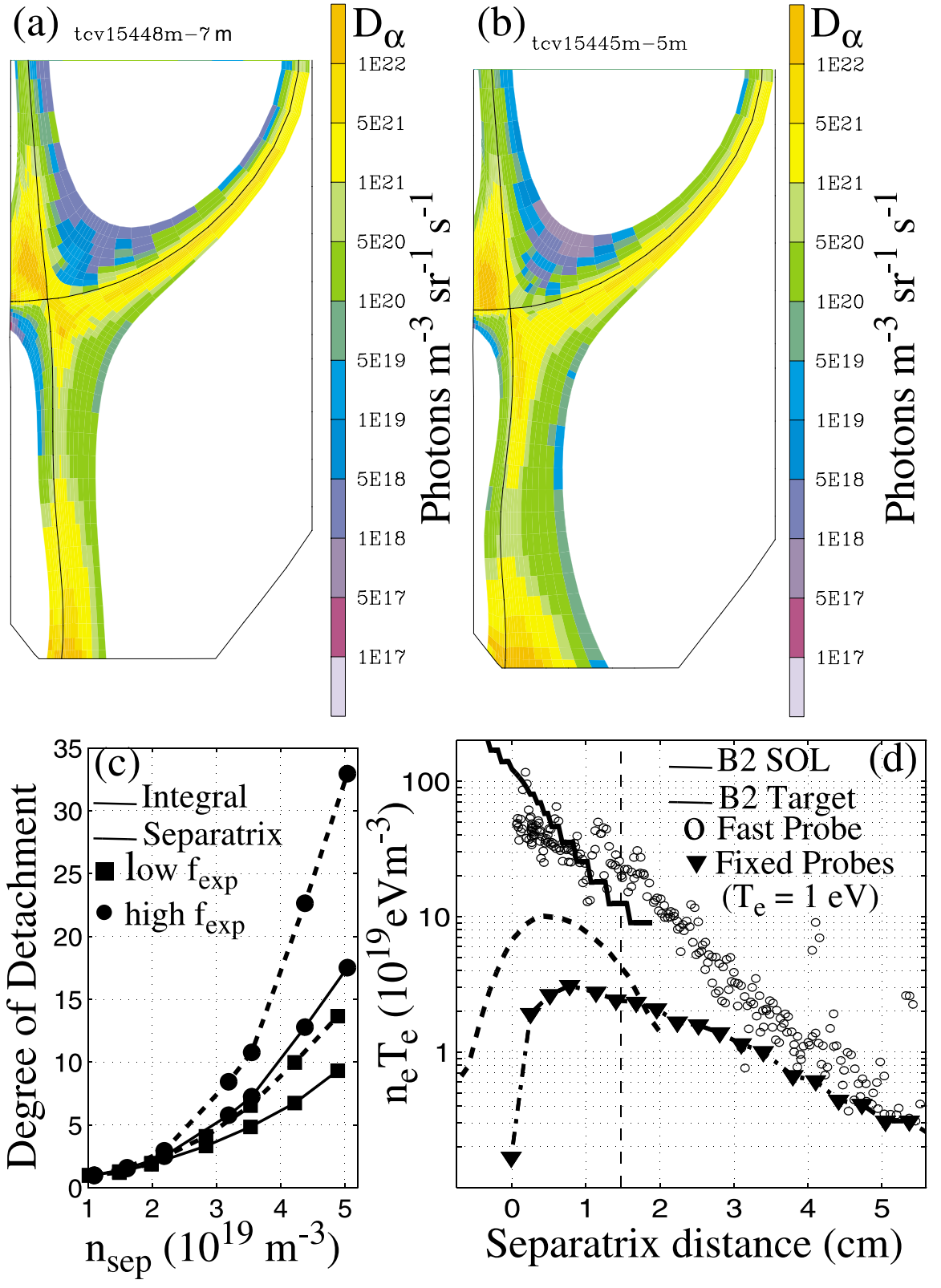
(a) tcv15448m−7 m
(b) tcv15445m−5m
Dα
1E22
5E21
1E21
5E20
1E20
5E19
1E19
5E18
1E18
5E17
1E17
Photons m-3 sr-1 s-1
(c)
Integral
Separatrix
low fexp
high fexp
Degree of Detachment
nsep (10^19 m^-3)
(d)
B2 SOL
B2 Target
Fast Probe
Fixed Probes
(Te = 1 eV)
ne Te (10^19 eVm^-3)
Separatrix distance (cm)

Fig. 5. Summary of selected B2-Eirene simulation results for the outer target and for low and high f_{exp} equilibria (TCV shots #15448, $f_{exp} = 2.8$ and #15445, $f_{exp} = 6.4$, $I_p = 345$ kA). The shapes of the D_α distributions in (a,b), shown for similar absolute recombination levels, are in good agreement with the experimental data (see Figs. 4(c) and (d)). In (c), separatrix and integral DODs for comparison with Fig. 3(d) code outer target pressure profiles during detachment compared with fast probe and target profile data at 1.0 s from Fig. 3. The target probe data have been corrected for the electron temperature ($T_e = 1$ eV) predicted by the code at these densities.

Finally, Fig. 5(d) compares the simulated SOL and target electron pressure profiles for low f_{exp} and under detached conditions. The experimental upstream data are replotted from Fig. 3 at $t = 1.0$ s, whilst the measured target pressure has been recomputed using the measured parallel ion flux, but replacing the experimental T_e with the fixed value of 1 eV across the target predicted by B2-Eirene at this density. Although theory and experiment do not coincide in absolute value, the *ratios* between upstream and target pressures in both cases are in very close agreement. This would seem to be a very convincing demonstration of the caution one should exercise in deriving T_e from target Langmuir probes under detached conditions. In the case of TCV at least, there are strong indications that this is largely due to the energy filtering action of the electrostatic sheath in selecting electrons originating from more distant zones in the plasma, where T_e is higher than the local value at the target.

5. Conclusions

This contribution has addressed the nature of plasma detachment in extremely open diverted configurations in the TCV tokamak, with emphasis on the effect of magnetic flux surface expansion at the outer target of deuterium fuelled ohmic discharges. Upstream and target Langmuir probe data, together with tomographically inverted visible CCD camera measurements of deuterium and carbon line emission are in good qualitative, and often quantitative, agreement with preliminary B2-Eirene code simulations demonstrating enhanced degrees of detachment as flux expansion is increased and clearly showing the effects of plasma plugging by expanded flux surfaces. Whilst the outer divertor, with high poloidal depth and a horizontal target, detaches readily, the inner divertor plasma, with X-point to target distances a factor of 7 shorter remains attached, except very close to the strike point, even at the highest densities. Comparison of code and experiment shows convincingly that target Langmuir probe measurements of local electron temperature can be in error by large factors under detached conditions.

Acknowledgements

CRPP would like to thank the Fusion Energy Program, University of California, San Diego, for the loan of the reciprocating probe. Thanks are also extended to B. Marletaz, P. Conti and P. Gorgerat of CRPP and L. Chousal and G. Gunner of UCSD for assistance and technical advice during its installation on TCV. This work was partly supported by the Fonds National Suisse de la Recherche Scientifique.

References

[1] O. Sauter et al., Phys. Rev. Lett. 84 (2000) 3322.
[2] R.A. Pitts et al., J. Nucl. Mater. 266–269 (1999) 648.
[3] R.A. Pitts, R. Chavan, J.-M. Moret, Nucl. Fus. 39 (1999) 1433.
[4] J.A. Boedo et al., Rev. Sci. Instrum. 69 (1998) 2663.
[5] A. Loarte et al., Nucl. Fus. 38 (1998) 331.
[6] B. Lipshultz et al., J. Nucl. Mater. 220–222 (1995) 50.
[7] T.W. Petrie et al., Nucl. Fus. 37 (1997) 321.
[8] N. Asakura et al., J. Nucl. Mater. 241–243 (1997) 559.
[9] M. Keilhacker et al., Phys. Scr. T2/2 (1982) 443.
[10] P.C. Stangeby, Plasma Phys. Contr. Fus. 37 (1995) 1459.
[11] J. Wesson, Plasma Phys. Contr. Fus. 37 (1995) 1031.
[12] J. Horacek, R.A. Pitts, A. Loarte, in preparation.
[13] M.E. Fenstermacher et al., Phys. Plasmas 4 (1997) 1761.
[14] B.P. Duval et al., Bull. Amer. Phys. Soc. 44 (1999) GP175.
[15] D. Reiter et al., Plasma Phys. Contr. Fus. 33 (1991) 1579.
[16] G. Haas et al., J. Nucl. Mater. 196–198 (1992) 481.
[17] U. Fantz et al., these Proceedings.